Investigation of the NADH/NAD$^+$ ratio in *Ralstonia eutropha* using the fluorescence reporter protein Peredox

Vijay Tejwani, Franz-Josef Schmitt, Svea Wilkening, Ingo Zebger, Marius Horch, Oliver Lenz, Thomas Friedrich

PII: S0005-2728(16)30653-3
DOI: doi:10.1016/j.bbabio.2016.11.001
Reference: BBABIO 47746

To appear in: *BBA - Bioenergetics*

Received date: 29 July 2016
Revised date: 11 October 2016
Accepted date: 2 November 2016

Please cite this article as: Vijay Tejwani, Franz-Josef Schmitt, Svea Wilkening, Ingo Zebger, Marius Horch, Oliver Lenz, Thomas Friedrich, Investigation of the NADH/NAD$^+$ ratio in *Ralstonia eutropha* using the fluorescence reporter protein Peredox, *BBA - Bioenergetics* (2016), doi:10.1016/j.bbabio.2016.11.001

Investigation of the NADH/NAD$^+$ ratio in *Ralstonia eutropha* using the fluorescence reporter protein Peredox

Vijay Tejwani, Franz-Josef Schmitt, Svea Wilkening, Ingo Zebger, Marius Horch, Oliver Lenz and Thomas Friedrich*

Technische Universität Berlin, Institut für Chemie, PC 14, Straße des 17. Juni 135, D-10623 Berlin, Germany

*corresponding author:
Phone: +49 (0)30 314 24128
Fax: +49 (0)30 314 78600
E-mail: friedrich@chem.tu-berlin.de

Keywords:
Ralstonia eutropha, fluorescence sensor protein, NADH/NAD$^+$ ratio, fluorescence lifetime, decay-associated spectra, hydrogenase

Abstract

Ralstonia eutropha is a hydrogen-oxidizing ("Knallgas") bacterium that can easily switch between heterotrophic and autotrophic metabolism to thrive in aerobic and anaerobic environments. Its versatile metabolism makes *R. eutropha* an attractive host for biotechnological applications, including H_2-driven production of biodegradable polymers and hydrocarbons. H_2 oxidation by *R. eutropha* takes place in the presence of O_2 and is mediated by four hydrogenases, which represent ideal model systems for both biohydrogen production and H_2 utilization. The so-called soluble hydrogenase (SH) couples reversibly H_2 oxidation with the reduction of NAD^+ to NADH and has already been applied successfully *in vitro* and *in vivo* for cofactor regeneration. Thus, the interaction of the SH with the cellular NADH/NAD^+ pool is of major interest. In this work, we applied the fluorescent biosensor Peredox to measure the [NADH]:[NAD^+] ratio in *R. eutropha* cells under different metabolic conditions. The results suggest that the sensor operates close to saturation level, indicating a rather high [NADH]:[NAD^+] ratio in aerobically grown *R. eutropha* cells. Furthermore, we demonstrate that multicomponent analysis of spectrally-resolved fluorescence lifetime data of the Peredox sensor response to different [NADH]:[NAD^+] ratios represents a novel and sensitive tool to determine the redox state of cells.

Introduction

Ralstonia eutropha H16 (renamed *Cupriavidus necator* in 2004) is a H_2-oxidizing β-proteobacterium ("Knallgas" bacterium) that populates soil and fresh water habitats at the aerobic-anaerobic interface. Due to its versatile metabolic features (Cramm, 2009; Jeffke et al., 1999; Lee et al., 2013; Schwartz et al., 2013), *R. eutropha* represents an attractive host and valuable model system for biotechnological applications. Since *R. eutropha* synthesizes polyhydroxyalkanoate (PHA) granules (Anderson and Dawes, 1990; Ishizaki et al., 2001), it has been extensively studied to optimize the production of biodegradable polymers (Reinecke and Steinbüchel, 2009). Furthermore, autotrophic growth of *R. eutropha* has been exploited for the biotechnological production of isopropanol (Torella et al., 2015). Moreover, the fundamental ability of *R. eutropha* to thrive on H_2 under aerobic conditions is of major interest in terms of future energy conversion approaches that utilize H_2 as a clean and renewable fuel.

In *R. eutropha*, the utilization of H_2 as the sole source of energy is mediated by four [NiFe]-hydrogenases that catalyse the reaction $H_2 \rightleftharpoons 2H^+ + 2e^-$, even at ambient O_2 levels (Lenz et al., 2015). Two of these enzymes are directly involved in providing energy and reductants for, e.g., CO_2 fixation through the Calvin-Benson-Bassham (CBB) pathway during lithoautotrophic growth (Friedrich et al., 1981). The membrane-bound hydrogenase (MBH) oxidizes H_2 in the periplasmic space and channels the electrons *via* a membrane-integral cytochrome *b* into the respiratory chain (Lenz et al., 2010), thereby generating a proton gradient over the cytoplasmic membrane. The cytoplasmic soluble hydrogenase (SH) couples directly H_2 oxidation with the reduction of NAD^+ to NADH. The latter is then used as a reductant in the CBB pathway and the respiratory chain (Schneider and Schlegel, 1976). The SH also catalyses the formation of H_2 from NADH to prevent 'over-reduction' of the cytoplasm under O_2-limiting conditions (Burgdorf et al., 2005). Thus, the SH is directly involved in biasing the cellular NAD(H) pool in response to the metabolic conditions. Conversely, the [NADH]:[NAD^+] ratio determines the catalytic direction of the SH and the structural and electronic properties of its redox cofactors (Horch et al., 2012). Thus, a technique for the determination of the [NADH]:[NAD^+] ratio in living cells is desirable to correlate the structural and functional state of the SH determined by *in vivo* spectroscopy (Horch et al., 2010) with the metabolic status of *R. eutropha* (Horch et al., 2015).

NAD^+ und NADH are pivotal cofactors for the cellular redox state, as determined by the [NADH]:[NAD^+] ratio. This ratio has been measured both in living and disrupted cells using fluorescence and chemical methods, which, in the latter case, indirectly estimate the free

NADH and NAD^+ concentrations from the concentration of redox couples such as lactate and pyruvate, whose ratio is determined by the lactate dehydrogenase reaction (Williamson et al., 1967). However, since this method involves cell lysis and a protein denaturation step, it does not necessarily reflect the situation in living cells. Moreover, since a substantial amount of NADH and NAD^+ is bound to proteins, it rather determines the total rather than the free NAD(H) concentration in the cytosol.

An alternative, non-invasive approach to monitor NADH and its phosphorylated form, NADPH, relies on the weak fluorescence of these compounds (Rocheleau et al., 2004). However, NADH and NADPH possess identical fluorescence spectra. Thus, quantitative discrimination between these two cofactors in living cells requires elaborate analyses based on fluorescence lifetime imaging (FLIM) and mathematical modelling (Blacker et al., 2014), and, since the corresponding oxidized forms, $NAD(P)^+$, are non-fluorescent, determination of the intracellular [NADH]:[NAD^+] ratio is impossible (Patterson et al., 2000).

Several genetically encoded fluorescent biosensors have been developed for the specific detection of the NADH level or the [NADH]:[NAD^+] ratio in living cells (Hung et al., 2011; Zhao et al., 2015; Zhao et al., 2011). In general, these sensors are constructed by fusing bacterial NADH-binding Rex repressor proteins to cyclically permuted fluorescent proteins (cpFPs) (Baird et al., 1999). Rex proteins are particularly sensitive to NADH binding (McLaughlin et al., 2010), which entails large conformational changes (McLaughlin et al., 2010; Wang et al., 2008). By fusing Rex proteins with cpFPs, the fluorescence of the latter responds to conformational changes induced by NADH binding (Baird et al., 1999).

The Peredox-mCherry sensor protein has been developed by fusing a cyclically permuted, monomeric T-Sapphire (cpmTS) as fluorescence reporter to a T-Rex tandem dimer (Hung et al., 2011). The red-fluorescent mCherry was fused to the C-terminus to enable normalization of the cpmTS fluorescence intensity with respect to the total concentration of the sensor protein. The Peredox sensor was mainly sensitive to the [NADH]:[NAD^+] ratio and resistant to pH changes or other metabolites with structural similarity to NADH. These properties qualify Peredox-mCherry as ideal for quantifying the redox status in as yet uncharacterized cellular environments.

In this work, we carried out spectrally resolved fluorescence lifetime measurements to characterize the response of Peredox to different $R' = \frac{1000 \times [\mathrm{NADH}]}{[\mathrm{NAD^+}]}$ and discuss its application as a probe for fluorescence lifetime imaging microscopy. Subsequently, we used Peredox-mCherry for the first time to measure the [NADH]:[NAD^+] ratio in bacterial cells, using *R. eutropha* as a model organism. The results suggest that the sensor operates close to saturation

level in aerobically grown *R. eutropha* cells indicating that the response parameter *R'* is larger than 15. The physiological implications of these findings and consequences for the successful application of Peredox-mCherry in bacterial cells are discussed.

Materials and Methods

All chemicals used in this study were at least at analytical grade. Sodium pyruvate, sodium DL-lactate, $FeCl_3 \cdot 6H_2O$, $NiCl_2$, NaCl, MOPS, KCl, $MgCl_2$, and glycerol were purchased from Sigma Aldrich (Deisenhofen, Germany). NAD^+, NADH disodium salt, and fructose were purchased from Applichem (Darmstadt, Germany), while $Na_2HPO_4 \cdot 2H_2O$, KH_2PO_4, NH_4Cl, $MgSO_4 \cdot 7H_2O$, and $CaCl_2 \cdot 2H_2O$ were obtained from Merck Millipore (Darmstadt, Germany). Oligonucleotide primers were ordered from Eurofins MWG Operon AG (Ebersberg, Germany).

Cloning of Peredox-mCherry in pET21b vector. The original plasmids harbouring Peredox-mCherry genes (pcDNA3.1-Peredox-mCherry and pRsetB-His7tag-Peredox-mCherry, the latter carrying an N-terminal 7×His tag) were purchased from Addgene (deposited from the lab of Gary Yellen, Harvard Medical School, USA)(Hung et al., 2011). The cDNA of Peredox-mCherry was cloned with a sequence encoding a C-terminal 7×His tag into pET21b between the restriction sites NdeI and XhoI by PCR using the following primers:

Forward primer: `5′-gagtatacatatgggtatgaaagttcctgaagcagc-3′`

Reverse primer: `5′-ccgtttgatctcgagtcaatgatgatgatgatggtgatgacccatcatttcttcgc-3′`

The pET21b vector encodes ampicillin resistance, and recombinant gene expression is controlled by a T7 promoter.

Cloning of the Peredox-mCherry gene into the pLO13-SH vector. The cDNA for Peredox-mCherry (without C-terminal His-tag-encoding sequence) was cloned into the pLO13-SH vector between the restriction sites NcoI and HindIII. To enable this cloning strategy, NcoI and HindIII restriction sites present within the Peredox-mCherry cDNA were eliminated by introducing silent mutations using the QuikChange site-directed mutagenesis kit (Agilent Technologies, Santa Clara, CA). The primers for PCR amplification were:

`5′gagtataccatgggcggcatgaaagttcctgaagcagccatttccagactgattacttac 3′ (forward)`

and `5′cttgataagctttcacttgtacagttcgtccatgccgcc 3′ (reverse)`

The pLO13-SH plasmid carries a tetracycline resistance gene, and expression of the Peredox-mCherry gene is based on the strong P_{SH} promoter of *Ralstonia eutropha* (Lauterbach and Lenz, 2013). The vector was transferred *via* conjugation into the host *R. eutropha* HF798 (SH^+, MBH^-, RH^-) using the donor *E. coli* strain S17-1 (Horch et al., 2010; Simon et al., 1983).

Expression and Purification of Peredox-mCherry. *E. coli* BL21(DE3) competent cells were transformed with the pET21b plasmid harbouring Peredox-mCherry and grown in 500 ml of LB medium containing 50 µg/mL of ampicillin at 37°C until OD_{600} reached 0.6. The cells were cooled down to room temperature, and expression was induced by addition of 0.5 mM IPTG for 16 hours at 18°C. The cells were harvested by centrifugation (8,000 g, 20 min), and the cell pellets were transferred to 50 mL conical tubes and stored at –80°C. The cell pellets were resuspended in 15 mL of lysis buffer (20 mM MOPS, 30 mM imidazole, 0.5 M NaCl) which also contained Complete® protease inhibitor (Roche Molecular Biochemicals, Mannheim, Germany). Cells were lysed by sonication (35 % amplitude, 50% on/off cycle) for 20 min on ice. After sonication, the lysate was centrifuged (10,000 g, 20 min, 4°C), and the top 12 mL representing the soluble fraction were collected. The soluble fraction was loaded onto a 1 mL HisTrap HP Ni-sepharose column (GE Healthcare, Freiburg, Germany). The flow-through was discarded and the column was washed with 4 column volumes of lysis buffer. The protein was eluted by a linear gradient of imidazole obtained using lysis and elution buffer (i.e., lysis buffer containing 350 mM imidazole), and the fractions with highest content of Peredox-mCherry protein were pooled. The eluted fractions were analysed by SDS-PAGE. Imidazole was removed from the pooled fraction by dialysis using MOPS buffer (100 mM MOPS, 50 mM KCl, 5 mM NaCl and 0.5 mM $MgCl_2$, pH 7.3). For long-term storage at -80°C, Peredox mCherry present in MOPS buffer was supplemented with 5% glycerol and snap-frozen in liquid N_2 for 5 min. The protein concentration was determined based on the absorbance at 280 nm, using the extinction coefficient of the apo-Peredox sensor (without NADH: 99,700 $M^{-1}\cdot cm^{-1}$) as calculated by ProtParam (http://web.expasy.org/protparam/).

Growth of *R. eutropha*. *R. eutropha* cells were grown in GN medium (24 mM $Na_2HPO_4\cdot 2H_2O$, 11 mM KH_2PO_4, 37 mM NH_4Cl, 0.81 mM $MgSO_4\cdot 7H_2O$, 68 µM $CaCl_2\cdot 2H_2O$, 11 µM $FeCl_3\cdot 6H_2O$, 1 µM $NiCl_2$, 0.4 % glycerol, pH 7.3) or FGN medium (GN medium containing 0.05 % (w/v) fructose) at 30°C. Cells were grown at 30°C in the presence of 10 µg/mL tetracycline to specified OD_{600} values (as indicated in figure legends and text).

Tetracycline has a strong fluorescence at above 500 nm (Schneider et al., 2003), which would interfere with emission of the cpmT-Sapphire sensor part of the Peredox-mCherry protein, and, consequently, it had to be removed for fluorescence measurements of living *R. eutropha* cultures. Therefore, cells were harvested by centrifugation (3,000 g for 10 min), and the pellet was resuspended in fresh GN medium to achieve a desired OD_{600} without antibiotic 30-60 min before measurements.

Gas bubbling of R. eutropha cell suspensions with H_2 and O_2. *R. eutropha* cell suspensions with an OD_{600} = 0.3 were bubbled with H_2 and O_2 in a 3 mL rubber stopper-sealed quartz cuvette with a rate of about 0.1 L/min at room temperature. The cuvettes were filled with 2 mL of cell suspension and bubbled slowly for the desired period of time. Subsequently, fluorescence spectra were recorded directly.

Permeabilization and lysis of R. eutropha cells. Several methods of cell permeabilization and lysis were tested to gain access to the intracellular content. Cells were grown in FGN medium to an OD_{600} of 3 and subsequently diluted with GN medium to an OD_{600} of 0.3. Methods tested were freeze-thawing (three cycles, either freezing in liquid N_2 for 5 min or in a −20°C freezer for 45 min followed by 5-min incubation at 37°C in a water bath), cell disruption in a glass beater (Disruptor Genie, VWR International GmbH, Darmstadt, Germany; 2:1 ratio of glass beads to cells, 5 min for three times at room temperature), and cell lysis using commercially available reagents (Easylyse™, Epicentre Technologies Corp.,Chicago, IL, or Bugbuster™, Merck Millipore, Darmstadt, Germany; both at 1.5% final concentration, 10 min incubation at room temperature). Furthermore, the cationic detergent cetyltrimethylammoniumbromide (CTAB; Sigma-Aldrich, Munich, Germany) was used to mildly permeabilize the cytoplasmic membrane of *R. eutropha* cells. This approach has been established previously (Eberz and Friedrich, 1991) and more recently applied for *in situ* spectroscopy of hydrogenases within *R. eutropha* cells (Horch et al., 2010). We found, however, that CTAB severely impedes Peredox fluorescence at concentrations necessary to achieve cell permeabilization (see Supplementary Information). Among the lysis methods tested, sonication was most efficient and preserved functionality of the Peredox protein. This was achieved by sonifying 25 mL of cell suspension (Branson SFX sonifier, Branson Ultrasonics, Danbury, CT; 35% amplitude, 50% on/off duty cycle) for 20 min on ice.

Estimation of the dilution factor in R. eutropha cell suspensions. Upon permeabilization of cell membranes or cell lysis, the small molecules in the cytoplasm were diluted by equilibration with the external medium. The dilution factor was estimated from the OD_{600} value assuming that *R. eutropha* cells are similar in size and shape to *E. coli* (spherocylinders with 0.9 µm diameter and 1.3 µm length (Makkar and Casida, 1987), yielding a cell volume of about 1 fL. An OD_{600} of 0.3 corresponds to 2.4×10^8 cells per mL, yielding a total cell volume of 0.24 µL per mL culture (http://www.genomics.agilent.com/biocalculators/calcODBacterial.jsp). Thus, the resulting dilution upon cell lysis should be about 4000-fold.

Ratiometric measurements. Fluorescence was measured with a Fluoromax-2 spectro-fluorometer (HORIBA Jobin Yvon GmbH, Bensheim, Germany). Peredox-mCherry was excited at 400 nm (cpmT-Sapphire sensor part of the protein) and 580 nm (mCherry part of sensor protein) separately. Emission spectra were recorded from 430 to 600 nm around the peak of the T-Sapphire emission (~ 510 nm), and from 590 nm to 680 nm around the peak of the mCherry emission (~ 610 nm), respectively, using a scan rate of 300 nm/min. All the measurements and dilutions were performed using GN buffer without tetracycline. The background from raw emission spectra of the cpmT-Sapphire band was subtracted by setting the lowest value in the spectra (at around 475 nm) to zero. The obtained spectra were then normalized by dividing the peak amplitude of the background-corrected Peredox emission spectrum by the peak amplitude (at ~ 610 nm) of the corresponding raw mCherry spectra. All experiments were carried out three times on independent biological samples. All errors are given as standard deviation.

Fluorescence Microscopy. A Nikon TI Eclipse wide-field fluorescence microscope equipped with 100× objective (N.A. 1.4) and a mercury lamp as light source was used for fluorescence imaging. Excitation of Peredox was performed with a dichroic filter cube containing a 405/20 bandpass excitation filter, a T 412 LPXT beam splitter and a 520/35 bandpass emission filter (all filters from AHF Analysentechnik, Tübingen, Germany). mCherry was excited *via* a dichroic filter cube containing a FB 550-40 bandpass filter (Thorlabs Inc., Newton, USA) and a T 560 LPXR beam splitter and observed *via* 570 long-pass or 605/55 bandpass filters (AHF Analysentechnik, Tübingen, Germany). Images were taken with an Andor Luca emCCD camera (Andor Technology Ltd., Belfast, UK).

Fluorescence Lifetime Imaging Microscopy (FLIM). A wide-field multi-parameter setup for fluorescence lifetime imaging microscopy was used with the same Nikon TI Eclipse microscope as described above and in (Schmitt et al., 2013; Schmitt et al., 2014). Excitation was performed with a 405 nm picosecond laser diode driven at 20 MHz (LDH-405, Picoquant, Berlin, Germany). The pulse train was focused on the back focal plane of the objective to achieve a uniform illumination of the whole field of view. A dichroic cube (488-DXCR, Cairn Research Limited, Faversham, UK) equipped with a 430 nm long-pass filter (AHF Analysentechnik, Tübingen, Germany) for blocking stray light from the laser and a bandpass filter (520/35, AHF Analysentechnik AG, Tübingen, Germany) were used to detect Peredox emission. Time- and space-resolved single photon counting for FLIM was performed using a novel time- and space-resolving multianode (MA) photomultiplier developed by the Leibniz Institute for Neurobiology, Magdeburg, Germany. The average lifetime of the fluorescence decay for spatially resolved FLIM pictures was calculated with the program QA analysis (EuroPhoton GmbH, Neusalza-Spremberg, Germany) and plotted in colour representation to show the spatial dependency of the fluorescence decay time. Single time-resolved fluorescence decay curves (Supplementary Figure 2) of purified Peredox protein were measured by applying the same excitation conditions and optical filter sets, but by using a crossed-delay-line single photon-counting detector (EuroPhoton GmbH, Neusalza-Spremberg, Germany).

Results

In vitro characterization of Peredox-mCherry. Peredox-mCherry was produced as C-terminally 7×His-tagged protein in BL21(DE3) cells and affinity purified using Ni-sepharose columns. The purified protein was characterized by fluorescence spectroscopy to investigate its *in vitro* response at different values of $R' = \frac{1000 \times [NADH]}{[NAD^+]}$, first, in the presence of 80 µM NAD^+ (for comparison with literature data) and, second, in the presence of 3 mM NAD^+, since intracellular concentrations at millimolar levels have been reported to be present in the cytoplasm of bacteria such as *E. coli* (Bennett et al., 2009; Zhou et al., 2011). The Peredox sensor emission spectra were normalized to the peak value of the corresponding mCherry emission spectrum for each titration condition to account for possible dilution effects, but the variations in the mCherry emission were very small (Supplementary Figure 1B,D). The Peredox sensor emission was smallest in the absence of nucleotides, and no change in amplitude was seen upon addition of 80 µM or 3 mM NAD^+ (Supplementary Figure 1A,C). Subsequent additions of NADH increased the sensor emission by up to a factor of 2.5 at *R'* values of 50 and higher, which is in line with previous reports (Hung et al., 2011).

Figure 1A,B shows the normalized amplitudes of the Peredox sensor emission dependent on *R'* for two different basal concentrations of NAD^+ (80 µM and 3 mM). Approximation of the data points with a Hill equation yielded $K_{R'}$ values (*R'* value for half-maximal sensor signal) of 5.8±0.4 for 80 µM NAD^+ and 3.9±1.2 for 3 mM NAD^+. The change of $K_{R'}$, observed upon increasing the total NAD(H) pool size, is in accordance with the results described by Hung *et al.* (Hung et al., 2011), and even a 37.5-fold increase in [NAD^+], covering the highest concentrations reported in bacteria (see (Bennett et al., 2009) and references therein), produced only a 30 % change in the $K_{R'}$ value. This shows that the sensor is still a good reporter, as long as the total NAD(H) pool does not drastically change *in vivo*. In addition, we also quantified the sensor's response to different NADH concentrations in the absence of NAD^+. Fitting a Hill equation to the normalized Peredox emission at NADH concentrations from 1 nM to 200 nM (Figure 1C), the half-maximal sensor response was found for an NADH concentration of 44.7±0.8 nM.

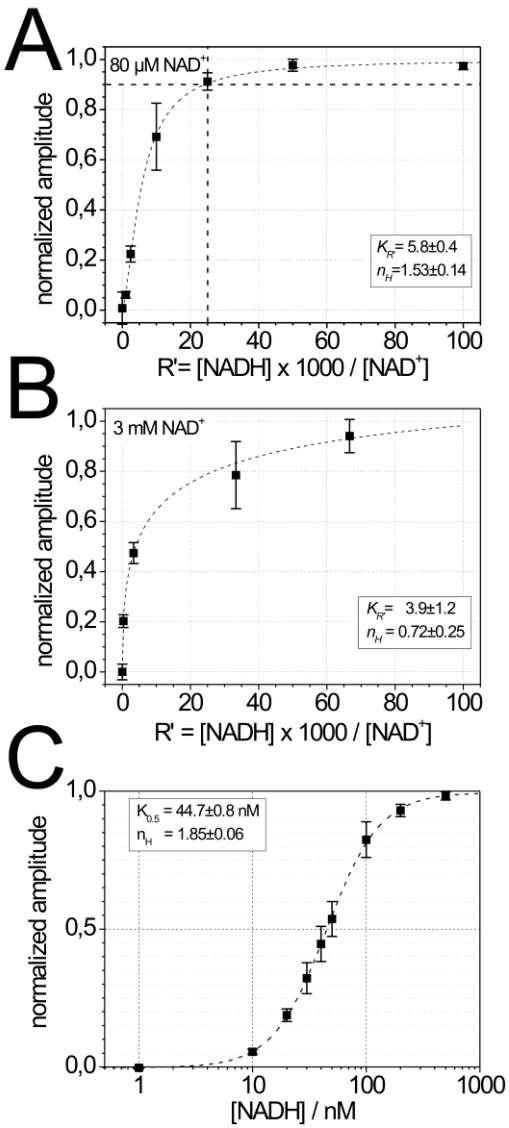

Figure 1: Dependence of normalized and background-subtracted Peredox sensor emission amplitudes on different $R' = \frac{1000 \times [NADH]}{[NAD^+]}$ (A and B) or [NADH] (C). Data from (A), measured at [NAD^+] = 80 µM, and (B), measured at [NAD^+] = 3 mM, were derived from the maxima (at 510 nm) of the Peredox sensor emission amplitudes (excitation at 400 nm) from three independent experiments as shown exemplarily in Supplementary Figure 1A and Supplementary Figure 1C, respectively, which were normalized to the corresponding maxima of the mCherry emission spectra in Supplementary Figure 1B and Supplementary Figure 1D, respectively. Subsequently, the minimum and maximum values of the normalized Peredox amplitudes were set to zero and 1, respectively, and all other amplitudes were scaled accordingly. (C) Dependence of the normalized, background-subtracted fluorescence emission amplitude of the purified Peredox-mCherry protein on [NADH], measured in the absence of NAD^+ (excitation at 400 nm), after scaling to values between zero and 1 as in (A) or (B). The superimposed curves were obtained from fitting a Hill function to the data, and the resulting fitting parameters are given in the insets. The horizontal and vertical dashed lines in (A) indicate the *R'* value corresponding to 90 % of maximal sensor response.

Evaluation of fluorescence analysis modes. Since measurements of the fluorescence intensity of the Peredox sensor emission in bacterial suspensions could be problematic due to the background of cellular autofluorescence or light scattering, we evaluated different fluorescence properties as a possible readout, which should enable an unambiguous discrimination of sensor signals from the cellular background. Thus, we measured the dependence of the Peredox sensor's fluorescence lifetime on *R'*, which, in principle, should show a similar ratio (about 2.5) between maximal and minimal sensor response. The fluorescence decay curves observed for purified Peredox-mCherry were found to exhibit a complex, multi-exponential behaviour and required at least two exponential components for satisfactory approximation (Supplementary Figure 2A,B). The average fluorescence lifetimes were 2.1 ns for Peredox (as purified) without NAD^+ or NADH, 2.9 ns with 15 µM NADH only, and values of 2.5 ns and 2.8 ns were measured for *R'* = 1 and *R'* = 25, respectively (Supplementary Figure 2C), showing that the average fluorescence lifetime only changes by about 40% between conditions of minimal and maximal sensor response. However, a more detailed analysis of the spectral dependence of the fluorescence decays (see Supplementary Methods) by calculating decay-associated spectra (DAS) showed that the fluorescence decays for all *R'* values tested comprise two components, a fast one of about 0.98 to 1.15 ns and a slower one of about 2.68 to 2.85 ns. The spectral shapes of both components resembled the shape of the Peredox emission spectrum (Supplementary Figure 3A-F). In these DAS, the relative contributions of the fast and slow spectral component varied characteristically with *R'*, as shown exemplarily in Supplementary Figure 3G for the data in the spectral channel around the emission maximum of Peredox (512.5±3.0 nm). These data show that the amplitude ratio $A(t_{fast}) / A(t_{slow})$ changed from 1.8 to 0.68 when *R'* was shifted from 1 to 50, at a basal NAD^+ concentration of 80 µM. Thus, the $A(t_{fast}) / A(t_{slow})$ ratio could serve as an equally sensitive quantity for the determination of *R'* as the fluorescence intensity ratio. Compared to intensity-based measurements, which can be done within a second, the recording of time-resolved fluorescence decays requires considerably longer acquisition times to resolve both decay (> 1 min) components with necessary precision. Thus, this approach might only be feasible under fairly stable steady-state conditions. Nonetheless, it provides a valuable alternative acquisition mode, for example in cases where (1) fluorescence intensity measurements are impeded by a complex (e.g., cellular) fluorescence background, or (2) if demultiplexing of different flurophores is required for the acquisition of several optical parameters, or (3) if the spectroscopy of Peredox must be done by evaluating only one emission wavelength.

Expression and Basic Response of Peredox-mCherry in R. eutropha. For production of Peredox-mCherry in *R. eutropha*, the sensor cDNA was cloned into the pLO13-SH vector, and the resulting plasmid was transferred by conjugation to *R. eutropha* strain HF798 (SH^+, MBH^-, RH^-) (Horch et al., 2010), which synthesizes the soluble hydrogenase, but not the membrane-bound and regulatory hydrogenases. Fluorescence imaging microscopy confirmed that the sensor protein was well expressed in the recombinant *R. eutropha* cells. Fluorescence was emitted by the whole cells in both detection channels (for Peredox and for mCherry) with distinctly bright spots close to the cell poles (Peredox sensor emission, green, and mCherry emission, red, Figure 2A,B). Fluorescence lifetime imaging microscopy on these samples (Figure 2C), however, revealed that there is a considerable variation of the average lifetime on a 1-2 ns time scale. This indicates that either the metabolic profile or the autofluorescence background might be variable between cells of the same population.

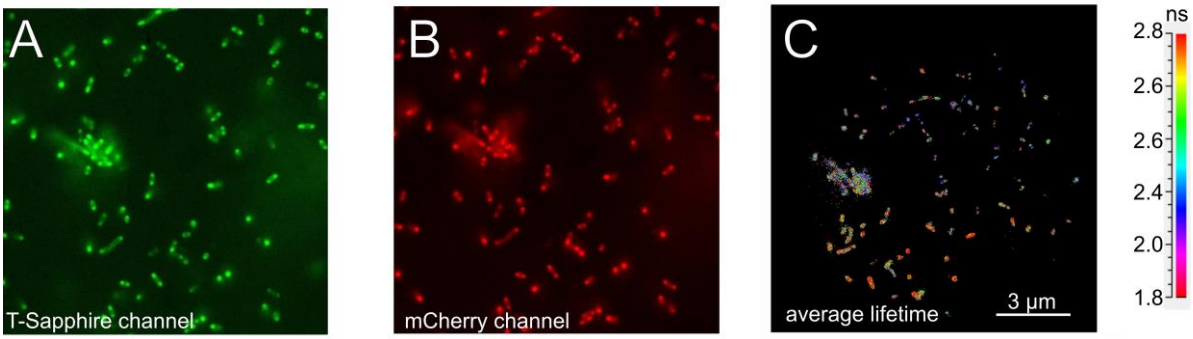

Figure 2: Fluorescence and fluorescence lifetime images of *R. eutropha* cells expressing the Peredox-mCherry sensor. (A) Peredox (cpmT-Sapphire) emission channel (excitation at 405 nm), (B) mCherry emission channel (excitation at 580 nm), (C) fluorescence lifetime image with average lifetimes depicted by color-coding as indicated by the scale on the right.

In vivo Response on Gaseous Substrates. We further sought to utilize the Peredox-mCherry sensor to monitor changes of the NAD(H) pool in suspensions of living *R. eutropha* cells, by changing the environmental conditions. The scattering background was eliminated from the raw fluorescence data by subtracting the minimum intensity value in the Peredox sensor emission spectrum at around 475 nm, and the peak amplitudes of the unprocessed mCherry emission spectra were subsequently used for normalization to account for differences in the protein synthesis level, cell density etc. First, emission spectra were recorded from aerobically grown cells (control) and, second, from cells of the same culture after bubbling with either H_2 or O_2 gas. As expected, bubbling the already aerobic sample with O_2 did not induce significant changes of the normalized Peredox sensor fluorescence (Figure 3A). In contrast, the change from aerobic to anaerobic, reducing conditions upon bubbling with H_2 should increase the NADH level due to the H_2-driven NAD^+ reduction by the SH and the

concomitant decrease of NADH consumption by the respiratory chain. Consequently, the normalized Peredox fluorescence was expected to increase. We observed, however, only a small signal gain of about 5-10% after 10 min of bubbling with H_2, which did not increase further with longer incubation times (Figure 3A,C). The mCherry signal remained fairly stable even over 30 min in both untreated and H_2-bubbled samples (Figure 3B,D). The fact that only a minor fluorescence increase was observed upon H_2 incubation might indicate that the sensor was already operating close to its NADH saturation level in aerobically grown *R. eutropha* cells.

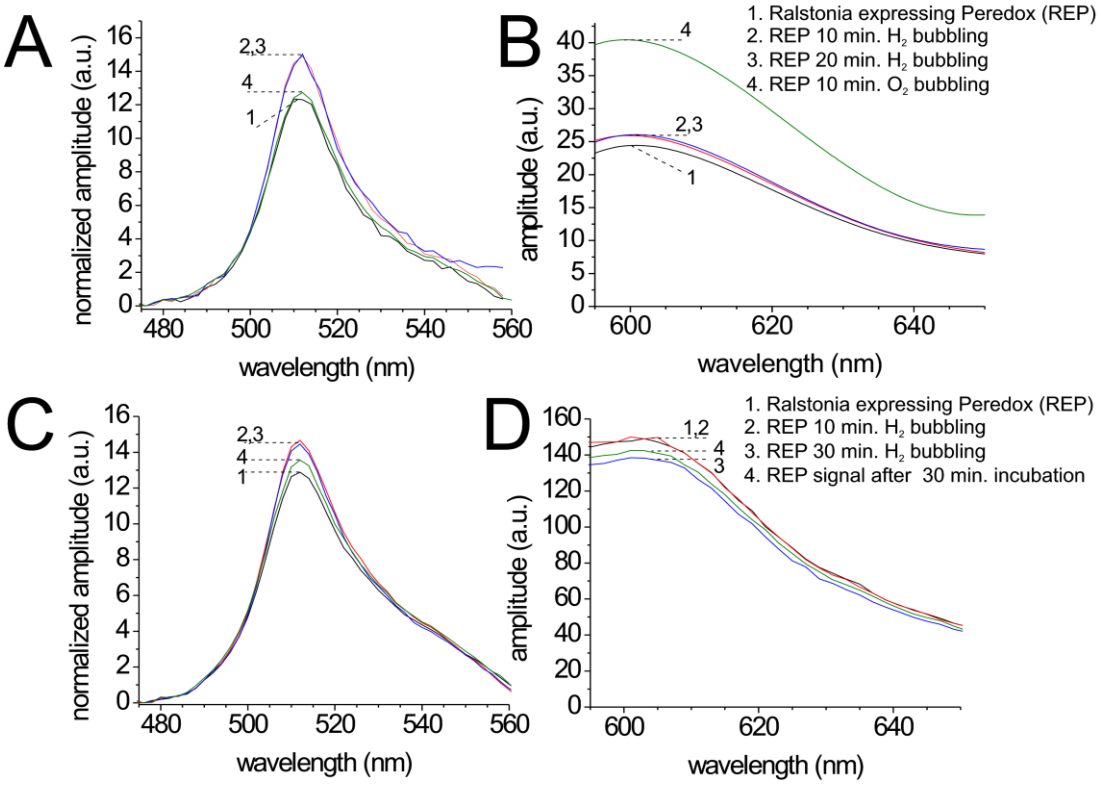

Figure 3: Effect of H_2 and O_2 incubation on the Peredox sensor response in *R. eutropha* cells. (A) Curves 1-4 show normalized, background-subtracted Peredox emission spectra (excitation at 400 nm), first, under aerobic conditions (curve 1, before H_2 bubbling), curves 2 and 3 after H_2 bubbling for 10 and 20 minutes, respectively, and curve 4 after bubbling cells with O_2 for 10 minutes. (B) shows the mCherry raw emission spectra corresponding to the data in (A) (excitation at 580 nm). (C) Curves 1-4 show normalized, background-corrected Peredox emission spectra (excitation at 400 nm), first, under aerobic conditions (curve 1, before H_2 bubbling), curves 2 and 3 after H_2 incubation for 10 and 30 minutes, respectively, and curve 4 shows the Peredox sensor response in the aerobic sample, which was kept for 30 min without gas treatment. (D) shows the mCherry raw emission spectra corresponding to the data in (C) (excitation at 580 nm). For (A,B) cells were grown in GN medium to OD_{600} of 0.8 and diluted to OD_{600} of 0.3 in fresh GN medium, only the O_2-incubated sample (curve 4) was kept at OD_{600} of 0.8, as indicated by the larger mCherry emission amplitude. For (C,D), cells were grown in FGN medium to OD_{600} of 3 and diluted to OD_{600} of 0.3 in fresh GN medium.

Determination of the R. eutropha Redox Status. To quantify the NAD(H) redox status of *R. eutropha*, we aimed to perform an *in vivo* calibration of the sensor by adding metabolites to the medium. As shown previously by Hung *et al.* (Hung et al., 2011), externally added substrates such as lactate and pyruvate were taken up by mammalian cells and shifted the intracellular NAD^+/NADH pool *via* the lactate dehydrogenase reaction. However, in the case of *R. eutropha* cells grown to OD_{600} of 3 in FGN medium, the fluorescence intensity of the Peredox sensor did not change within 10 min upon addition of either of NADH (1 µM), NAD^+ (100 µM), lactate (10 mM), pyruvate (10 mM) or fructose (10 mM) to the medium (data not shown).

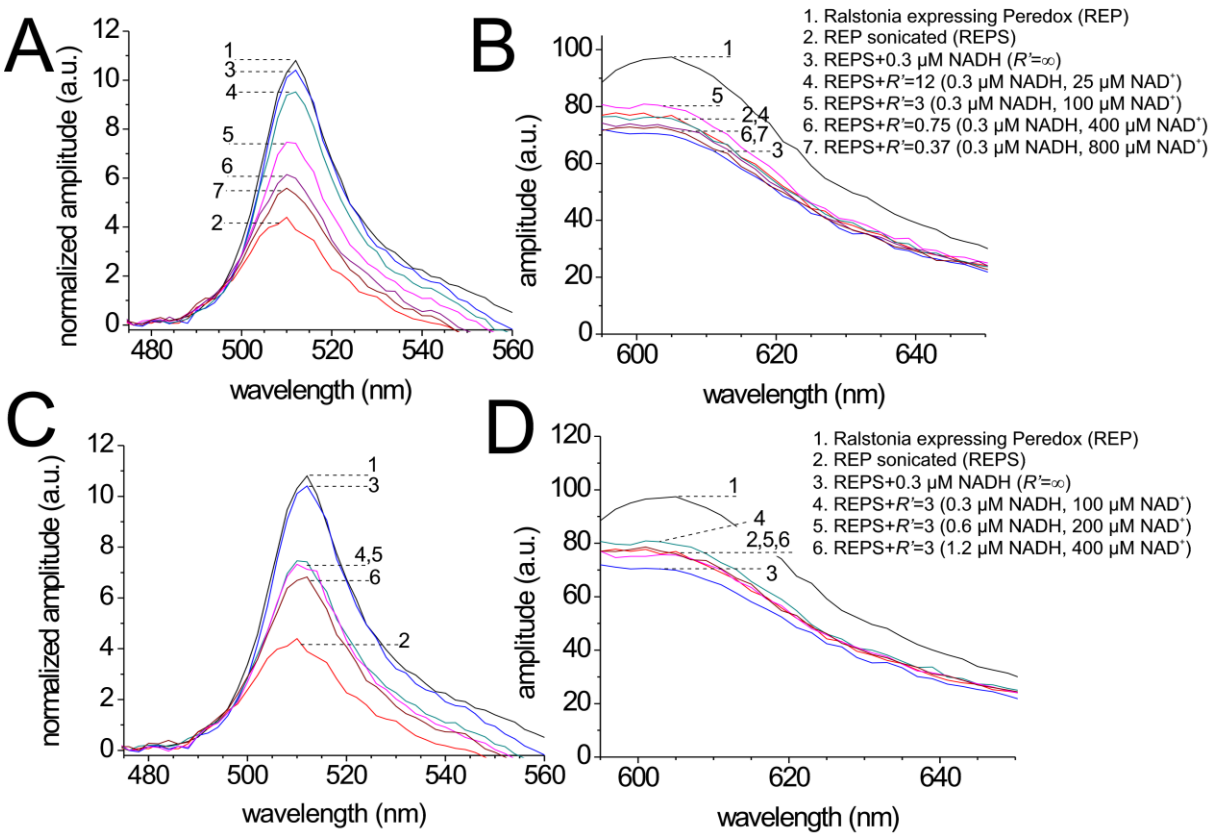

Figure 4: Response of Peredox-mCherry sensor in intact *R. eutropha* cells and upon lysis by sonication and subsequent addition of different NADH and NAD^+ concentrations.
(A) Background-subtracted and normalized Peredox emission spectra (excitation at 400 nm) before/after cell lysis and in response to different $R' = \frac{1000 \times [NADH]}{[NAD^+]}$.
(B) Corresponding mCherry raw emission spectra (excitation at 580 nm).
(C) Background-subtracted and normalized Peredox emission spectra (excitation at 400 nm) before/after cell lysis and at $R' = 3$ with different concentrations of NADH/NAD^+.
(D) Corresponding mCherry raw emission spectra (excitation at 580 nm). Cells were grown to OD_{600} of 2 in FGN medium and diluted to OD_{600} of 0.3 in fresh GN medium.

In order to establish an „*ex vivo*“ calibration of the Peredox sensor in *R. eutropha*, we next evaluated various cell lysis methods to release the protein from the cells and test its

functionality. *R. eutropha* cells were grown to OD_{600} of 2 and resuspended in GN medium to yield an OD_{600} of 0.3, which was suitable for measurements. We tested whether the released sensor responded reasonably to varying concentrations of NADH and NAD^+ (*R'* values) to enable calibration and ultimately obtain an estimate of the *R'* value for intact *R. eutropha* cells. From the lysis methods tested (freeze-thaw cycles, lysozyme treatment, glass beater, commercial lysis solutions containing detergents, sonication), only sonication preserved the responsiveness of the Peredox sensor to NADH and different *R'* values (Figure 4). Figure 4A shows that the high amplitude of the normalized Peredox fluorescence measured for the untreated sample decreased upon lysis to about 40 % of the initial amplitude, which is in line with an about 4000-fold dilution of cellular constituents under these conditions (see Materials and Methods section for an estimation of the dilution factor from the OD_{600} value of a *R. eutropha* culture). Upon lysis, also the mCherry fluorescence amplitude decreased by about 20 %, which could be due to the altered turbidity of the probes and different scattering properties. Addition of 0.3 µM NADH to the lysed sample led to an increase of the Peredox fluorescence to nearly the same amplitude as measured for untreated cells (Figure 4A), indicating again that the sensor response in intact cells was already close to maximum (at negligible NAD^+ concentrations, 0.3 µM NADH formally corresponds to $R' = \infty$, see also Figure 1C). An increase of the NAD^+ concentration in the presence of 0.3 µM NADH revealed a gradual decrease of the Peredox response (Figure 4A), with a similar dependence on *R'* as measured for the purified sensor protein (*in vitro*, Figure 1A,B). Consistently, addition of 1.2 µM NADH to the lysed sample fully restored the original Peredox sensor amplitude measured in untreated cells, and decreasing amounts of NADH in the concomitant presence of a high NAD^+ concentration (800 µM) gradually lowered the response (data not shown). To test the robustness of the sensor at around its $K_{R'}$ in the lysate, we also added three different concentrations of NADH and NAD^+, always at the same *R'* value of 3 (Figure 4C). Here, two- and three-fold increases in the concentrations of NADH and NAD^+ gave very similar sensor responses if *R´* was not changed. This is in agreement with observations by Hung *et al.* (Hung et al., 2011), where an up to three-fold increase in the total NADH/NAD^+ pool hardly affected the sensor response (as reflected by $K_{R'}$).

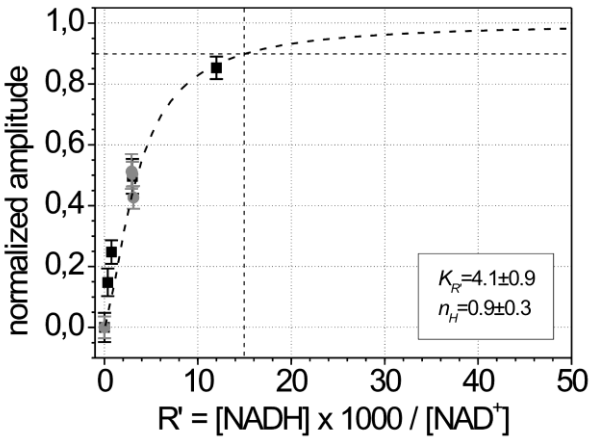

Figure 5: *"Ex vivo"* response curve of the Peredox-mCherry sensor upon lysis of *R. eutropha* cells by sonication. The data were derived from the two types of experiments as shown exemplarily in Figure 4. Symbols indicate the Peredox emission amplitudes, which were normalized to the corresponding maxima of the mCherry emission spectra. Subsequently, the minimum (Peredox fluorescence amplitude after cell lysis, plotted as zero normalized amplitude at $R' = 0$) and maximum (Peredox amplitude after cell lysis and addition of 0.3 µM NADH) values of the normalized Peredox amplitudes were set to zero and 1, respectively, and all other amplitudes were scaled accordingly. Black symbols: normalized Peredox response measured after cell lysis in response to different $R' = \frac{1000 \times [NADH]}{[NAD^+]}$ (at [NADH] = 0.3 µM, referring to data as shown Fig. 4A), grey symbols: normalized Peredox responses at $R' = 3$ with different concentrations of NADH/NAD^+ (referring to data as shown in Figure 4C). The superimposed curve corresponds to the result of fitting a Hill function to the whole data set; fitting parameters are given in the inset. The horizontal and vertical dashed lines indicate the *R'* value corresponding to 90 % of maximal sensor response.

The normalized Peredox fluorescence amplitudes measured after cell lysis in response to different *R'* values from three experiments (one dataset shown exemplarily in Figure 4) yield the "*ex vivo*" response curve depicted in Figure 5, which corresponds well with the response curves of the purified Peredox protein to different *R'* values from Figure 1. Based on the premise that the Peredox signal amplitude in aerobically grown *R. eutropha* corresponds to about 90 % of its maximum (from the 10% increase observed upon H_2 bubbling), an *R'* value of greater than 15 results from the "*ex vivo*" response curve in Figure 5, while a value of *R'* greater than 25 is derived from the calibration curve of the purified sensor in Figure 1A. Figure 1B appears to indicate an even more reduced NAD(H) pool; however, this finding may suffer from less accurate fluorescence estimates for high *R'*. Thus, a conservative estimation based on the lower of the two aforementioned values indicates that the *R'* value in the cytoplasm of *R. eutropha* must be greater than 15.

Discussion

Knowledge about the distribution and concentration of metabolites is of key importance for understanding biochemical processes in cells and for determining changes due to pathological processes, environmental factors, and human intervention. Metabolite detection frequently uses enzymatic assays, chromatography, mass spectrometry or NMR spectroscopy (Lenz and Wilson, 2007); however, since these techniques imply sample destruction, non-invasive techniques like fluorescence monitoring are required to achieve real-time and space-resolved metabolite analytics in living cells.

So far, studies using the latter strategy have largely focused on mammalian cells. Using *R. eutropha* as a model organism, we utilized the fluorescence sensor protein Peredox, for the first time, to determine the cellular redox state of a bacterium. In the particular case of *R. eutropha*, the application of such sensors should ultimately allow correlating the cellular [NADH]:[NAD^+] ratio with the structural and functional state of its NAD^+-reducing soluble hydrogenase *in vivo*. This approach may provide valuable information to promote the development of sustainable strategies for cell-based biohydrogen production or nucleotide cofactor regeneration with this enzyme (Horch et al., 2012; Lauterbach et al., 2013).

Starting with a detailed *in vitro* characterization of Peredox, we explored different fluorescence analysis modes that extend the basic ratiometric readout applied by Hung *et al.* (Hung et al., 2011). Analysis of the fluorescence signals of the response of purified Peredox to different [NADH] and [NAD^+] by time-correlated single-photon counting revealed that the lifetime changes from 2.1 ns (in the absence of NAD^+ and NADH) to 2.9 ns (in the presence of 15 µM NADH). This is in good agreement with a recent study (Mongeon et al., 2016), in which two-photon excitation and fluorescence lifetime imaging microscopy (FLIM) has been used to determine the [NADH]:[NAD^+] ratio in neurons and astrocytes of mouse hippocampal brain slices. An average lifetime of purified Peredox protein ranging between 1.6 ns (at *R'* values below about 0.1) and 2.6 ns (at *R'* values above 10) was reported. Since fluorescence lifetime is absolutely calibrated and independent of sensor concentration, quantitative assessment of the NAD(H) redox state by FLIM would therefore allow for an absolute measurement of the [NADH]:[NAD^+] ratio in living cells.

Extending this analysis by time- and wavelength-resolved fluorescence spectroscopy, we found that the fluorescence decay of Peredox is characterized by two components with lifetimes of about 1.1 ns and 2.8 ns. Both components have similar spectral signatures indicating two spectrally indistinguishable chromophore states that decay with different time constants (Supplementary Figure 3). With increasing $R' = \frac{1000 \times [\mathrm{NADH}]}{[\mathrm{NAD^+}]}$, the relative

contribution of the slow component increased and the fast component decreased, and the amplitude ratio $A(\tau_{fast})/A(\tau_{slow})$ is an equally sensitive criterion for [NADH]:[NAD^+] quantification as the conventional ratiometric readout, which also offers a larger dynamic range (about 260%) than analyses based on determining the average fluorescence lifetime (about 150%). Thus, in line with the study by (Mongeon et al., 2016), fluorescence lifetime analysis based on the Peredox fluorescence alone is suitable for the determination of the [NADH]:[NAD^+] ratio and obviates the necessity to use the mCherry signal as a normalization standard. However, since the acquisition of fluorescence lifetime spectra/images lasts over minutes and requires extensive after-processing of the data, this application is best suited for steady-state monitoring. Under changing conditions, however, fast measurements, such as the ratiometric readout based on fluorescence intensities, are preferable. Hence, we used the latter method in all subsequent experiments.

For *in vivo* studies, Peredox-mCherry was robustly expressed in recombinant *R. eutropha* cells. Surprisingly, experiments with living *R. eutropha* cells revealed that the transition from aerobic, oxidizing to anaerobic, reducing conditions caused by incubation with H_2 gas was accompanied by only minor increases in Peredox sensor emission, which did not reflect the expected temporary rise in NADH concentration. *Ex vivo* experiments on cells lysed by sonication allowed a correlation of the sensor's fluorescence emission before/after lysis with its response upon exposure of the lysate to defined *R'* values. Notably, the high Peredox emission amplitude measured in living *R. eutropha* cells could only be reproduced with cell lysates upon addition of NADH alone. This observation shows that the sensor is operating in living cells at its saturation level, which explains why the incubation of aerobically grown cells with H_2 gas caused only a small increase in the sensor response. Based on the *"ex vivo"* response curve from Figure 5, the *R'* value in aerobically grown *R. eutropha* cells must be larger than 15, as estimated from the *R*' values corresponding to 90 % of the maximum sensor signal. From these results, the NAD^+ and NADH concentrations present in aerobically grown cells can be estimated. Here, we consider (1) an about 4000-fold dilution of the cytoplasm upon cell lysis under our measurement conditions (see Materials and Methods section), (2) the observation that the sensor response dropped to its minimum upon cell lysis (Figure 4), and (3) an [NADH] for half-maximal sensor response ($K_{0.5}$) of about 44.7 nM (Figure 1C). Based on these premises, the NADH concentration in the lysate might not be larger than 7 nM, if a normalized sensor fluorescence of 3 % from maximum is considered as the lower limit of detection. This corresponds to about 28 µM free cytosolic NADH, and from the estimated *R'* value of ≈ 15, the corresponding free cytosolic [NAD^+] would be ≈ 1.9 mM.

R' values in mammalian cells vary according to cell types or metabolic challenge. Using Peredox, Hung and coworkers reported [NAD^+]:[NADH] (= 1000/*R'*) values of about 300 (corresponding to *R'* = 3.3) for mouse neuroblastoma Neuro-2a and rat glioma S6 cancer cells in the absence of external glucose, but *R'* increased to between 6 and 14 upon glucose supply (Hung et al., 2011). These authors also found that astrocytes had a more reduced redox state, with an *R'* of about 12 compared to neurons (*R'* of about 8) under glucose supply. Estimates for normal tissue cells revealed *R'* values of 1.4 to 5 (Williamson et al., 1967) suggesting them to be more oxidized than cancer cells, which is in line with the expectation that cancer cells perform intense aerobic glycolysis, as mentioned earlier by (Warburg, 1956). In another study, two-photon fluorescence lifetime imaging on normal and cancer breast cells revealed an average intracellular [NADH] of ~100 µM and ~170 µM, respectively, whereby the dominant NADH autofluorescence signal originated from mitochondria (Yu and Heikal, 2009). From NADH fluorescence anisotropy analysis, the same authors also inferred that in normal cells only about 20 % of the total cellular NADH content are in the free state and the rest remained bound to proteins, which is consistent with similar findings for mitochondria (Blinova et al., 2005).

Gram-negative bacteria such as *E. coli* are known to possess cytoplasmic NAD^+ and NADH concentrations in the low millimolar range. Based on a cofactor recycling assay with cell lysates (Zhou et al., 2011), the aerobically grown wild-type strain *E. coli* BW25113 has been reported to possess total NAD^+ and NADH concentrations of 0.64 mM and 0.24 mM, respectively, which corresponds to an *R'* of about 375. The same study also reported for the NAD^+-auxotrophic mutant, *E. coli* YJE003, total NADH concentrations ranging between 0.020 and 0.99 mM when supplemented with [NAD^+] of 0.019 – 7.5 mM (*R'* between 130 and 275). Using liquid chromatography-tandem mass spectrometry, Bennett *et al.* determined the total concentrations of NADH and NAD^+ from extracts from glucose-fed, exponentially grown *E. coli* cells under aerobic conditions (Bennett et al., 2009). A [NADH] of 83 µM and a [NAD^+] of 2.55 mM was measured, which converts into an *R'* of about 32.5. This method, however, did not differentiate between free and protein-bound NAD(H) since the proteins had been denatured by organic solvent during the extraction step. Consistently, our estimated values of 28 µM and about 1.9 mM for free cytosolic NADH and NAD^+, respectively, in *R. eutropha* are considerably smaller. Assuming that the total NADH concentration also in *R. eutropha* cells is five times greater than the concentration of free NADH (Blinova et al., 2005), total [NADH] and [NAD^+] would be 140 µM and 9.5 mM, respectively, which does not largely exceed the aforementioned values from other bacteria. In summary, previous data

suggest that bacteria have a significantly more reduced [NADH]:[NAD^+] ratio than mammalian cells, and the results from our study support this notion for *Ralstonia eutropha*. Although Peredox-mCherry possesses several advantages with regard to its application in as yet uncharacterized cell lines, it is certainly not the optimal reporter protein for evaluating the NAD(H) redox state in bacteria. Besides its high NADH affinity, difficulties have been reported in terms of slow responsiveness and its rapid saturation with NADH *in vivo* (Zhao et al., 2015). Another study reported that Peredox failed in responding adequately to [NADH]:[NAD^+] changes in mitochondria, which has also been explained by its high affinity towards NADH (Bilan et al., 2014). Thus, further efforts in genetic engineering are required to generate a toolkit of Peredox sensor variants with NADH sensitivity adapted to the particular cellular or organelle system to be studied.

Highlights

- The fluorescent sensor protein Peredox, which is composed of a cyclically-permuted T-sapphire fused to a tandem dimer of the bacterial NADH-binding Rex repressor from *Thermus aquaticus*, was utilized for the first time to measure the [NADH]:[NAD^+] ratio in a bacterial model organism of high biotechnological potential, *Ralstonia eutropha*.
- The Peredox sensor, which had been developed for applications in mammalian cells, operates close to its saturation level in aerobically grown *R. eutropha* cells indicating a rather high [NADH]:[NAD^+] ratio.
- By comparing the *in vivo* response of Peredox to signals measured in acutely prepared lysates of *R. eutropha* cells, we arrive at estimations of 28 µM and about 1.9 mM for the free cytosolic NADH and NAD^+ concentrations in *R. eutropha*, respectively.
- Multicomponent analysis of spectrally resolved fluorescence lifetime data represents a novel tool for determining [NADH]:[NAD^+], which is equally or even more sensitive than conventional ratiometric readout.

Conflict of interests statement

The authors declare that there are no conflicts of interest.

Acknowledgements

The authors acknowledge support by the German Research Foundation DFG (cluster of excellence „Unifying Concepts in Catalysis“) and the Leibniz Institute for Neurobiology (Magdeburg, Germany) for providing a novel multi-anode wide-field FLIM detector.

References

Anderson, A.J. and Dawes, E.A. (1990) Occurrence, metabolism, metabolic role, and industrial uses of bacterial polyhydroxyalkanoates. *Microbiol. Rev.*, **54**, 450-472.

Baird, G.S., Zacharias, D.A. and Tsien, R.Y. (1999) Circular permutation and receptor insertion within green fluorescent proteins. *Proc. Natl. Acad.Sci. U. S. A.*, **96**, 11241-11246.

Bennett, B.D., Kimball, E.H., Gao, M., Osterhout, R., Van Dien, S.J. and Rabinowitz, J.D. (2009) Absolute metabolite concentrations and implied enzyme active site occupancy in *Escherichia coli*. *Nat. Chem. Biol.*, **5**, 593-599.

Bilan, D.S., Matlashov, M.E., Gorokhovatsky, A.Y., Schultz, C., Enikolopov, G. and Belousov, V.V. (2014) Genetically encoded fluorescent indicator for imaging NAD^+/NADH ratio changes in different cellular compartments. *Biochim. Biophys. Acta*, **1840**, 951-957.

Blacker, T.S., Mann, Z.F., Gale, J.E., Ziegler, M., Bain, A.J., Szabadkai, G. and Duchen, M.R. (2014) Separating NADH and NADPH fluorescence in live cells and tissues using FLIM. *Nat. Commun.*, **5**, 3936.

Blinova, K., Carroll, S., Bose, S., Smirnov, A.V., Harvey, J.J., Knutson, J.R. and Balaban, R.S. (2005) Distribution of mitochondrial NADH fluorescence lifetimes: steady-state kinetics of matrix NADH interactions. *Biochemistry*, **44**, 2585-2594.

Burgdorf, T., Lenz, O., Buhrke, T., van der Linden, E., Jones, A.K., Albracht, S.P.J. and Friedrich, B. (2005) [NiFe]-Hydrogenases of *Ralstonia eutropha* H16: Modular Enzymes for Oxygen-Tolerant Biological Hydrogen Oxidation. *J. Mol. Microbiol. Biotechnol.*, **10**, 181-196.

Cramm, R. (2009) Genomic view of energy metabolism in *Ralstonia eutropha* H16. *J. Mol. Microbiol. Biotechnol.*, **16**, 38-52.

Eberz, G. and Friedrich, B. (1991) Three trans-acting regulatory functions control hydrogenase synthesis in *Alcaligenes eutrophus*. *J. Bacteriol.*, **173**, 1845-1854.

Friedrich, C.G., Friedrich, B. and Bowien, B. (1981) Formation of Enzymes of Autotrophic Metabolism During Heterotrophic Growth of *Alcaligenes eutrophus*. *Microbiology*, **122**, 69-78.

Horch, M., Hildebrandt, P. and Zebger, I. (2015) Concepts in bio-molecular spectroscopy: vibrational case studies on metalloenzymes. *Phys. Chem. Chem. Phys.*, **17**, 18222-18237.

Horch, M., Lauterbach, L., Lenz, O., Hildebrandt, P. and Zebger, I. (2012) NAD(H)-coupled hydrogen cycling - structure-function relationships of bidirectional [NiFe] hydrogenases. *FEBS Lett.*, **586**, 545-556.

Horch, M., Lauterbach, L., Saggu, M., Hildebrandt, P., Lendzian, F., Bittl, R., Lenz, O. and Zebger, I. (2010) Probing the active site of an O_2-tolerant NAD^+-reducing [NiFe]-hydrogenase from *Ralstonia eutropha* H16 by in situ EPR and FTIR spectroscopy. *Angew. Chem. Int. Ed. Engl.*, **49**, 8026-8029.

Hung, Y.P., Albeck, J.G., Tantama, M. and Yellen, G. (2011) Imaging cytosolic NADH-NAD^+ redox state with a genetically encoded fluorescent biosensor. *Cell Metab.*, **14**, 545-554.

Ishizaki, A., Tanaka, K. and Taga, N. (2001) Microbial production of poly-D-3-hydroxybutyrate from CO_2. *Appl. Microbiol. Biotechnol.*, **57**, 6-12.

Jeffke, T., Gropp, N.H., Kaiser, C., Grzeszik, C., Kusian, B. and Bowien, B. (1999) Mutational analysis of the cbb operon (CO_2 assimilation) promoter of *Ralstonia eutropha*. *J. Bacteriol.*, **181**, 4374-4380.

Lauterbach, L. and Lenz, O. (2013) Catalytic production of hydrogen peroxide and water by oxygen-tolerant [NiFe]-hydrogenase during H_2 cycling in the presence of O_2. *J. Am. Chem. Soc.*, **135**, 17897-17905.

Lauterbach, L., Lenz, O. and Vincent, K.A. (2013) H_2-driven cofactor regeneration with $NAD(P)^+$-reducing hydrogenases. *Febs J.*, **280**, 3058-3068.

Lee, J.W., Brigham, C.J., Gai, C.S., Lu, J., Speth, D.R., Worden, R.M. and Sinskey, A.J. (2013) Engineering *Ralstonia eutropha* for Production of Isobutanol from CO_2, H_2, and O_2. In *Advanced Biofuels and Bioproducts*. Springer New York, pp. 1065-1090.

Lenz, E.M. and Wilson, I.D. (2007) Analytical Strategies in Metabonomics. *J. Proteome Res.*, **6**, 443-458.

Lenz, O., Lauterbach, L., Frielingsdorf, S. and Friedrich, B. (2015) Oxygen-tolerant hydrogenases and their biotechnological potential. In Rögner, M. (ed.), *Biohydrogen*. De Gruyter, Berlin, pp. 61-96.

Lenz, O., Ludwig, M., Schubert, T., Bürstel, I., Ganskow, S., Goris, T., Schwarze, A. and Friedrich, B. (2010) H_2 Conversion in the Presence of O_2 as Performed by the Membrane-Bound [NiFe]-Hydrogenase of *Ralstonia eutropha*. *ChemPhysChem*, **11**, 1107-1119.

Makkar, N.S. and Casida, L.E. (1987) *Cupriavidus necator* gen. nov., sp. nov.: a Nonobligate Bacterial Predator of Bacteria in Soil. *Int. J. Syst. Bact.*, **37**, 323-326.

McLaughlin, K.J., Strain-Damerell, C.M., Xie, K., Brekasis, D., Soares, A.S., Paget, M.S. and Kielkopf, C.L. (2010) Structural basis for $NADH/NAD^+$ redox sensing by a Rex family repressor. *Mol. Cell*, **38**, 563-575.

Mongeon, R., Venkatachalam, V. and Yellen, G. (2016) Cytosolic $NADH\text{-}NAD^+$ Redox Visualized in Brain Slices by Two-Photon Fluorescence Lifetime Biosensor Imaging. *Antioxid. Redox Signal.*, Epub ahead of print.

Patterson, G.H., Knobel, S.M., Arkhammar, P., Thastrup, O. and Piston, D.W. (2000) Separation of the glucose-stimulated cytoplasmic and mitochondrial NAD(P)H responses in pancreatic islet beta cells. *Proc. Natl. Acad. Sci. U. S. A.*, **97**, 5203-5207.

Reinecke, F. and Steinbüchel, A. (2009) *Ralstonia eutropha* Strain H16 as Model Organism for PHA Metabolism and for Biotechnological Production of Technically Interesting Biopolymers. *J. Mol. Microbiol. Biotechnol.*, **16**, 91-108.

Rocheleau, J.V., Head, W.S. and Piston, D.W. (2004) Quantitative NAD(P)H/flavoprotein autofluorescence imaging reveals metabolic mechanisms of pancreatic islet pyruvate response. *J. Biol. Chem.*, **279**, 31780-31787.

Schmitt, F.J., Maksimov, E.G., Junghans, C., Weißenborn, J., Hätti, P., Paschenko, V.Z., Allakhverdiev, S.I. and Friedrich, T. (2013) Structural Organization and Dynamic Processes in Protein Complexes Determined by Multiparameter Imaging. *NanoPhotoBiosciences*, **1**, 1-45.

Schmitt, F.J., Thaa, B., Junghans, C., Vitali, M., Veit, M. and Friedrich, T. (2014) eGFP-pHsens as a highly sensitive fluorophore for cellular pH determination by fluorescence lifetime imaging microscopy (FLIM). *Biochim. Biophys. Acta*, **1837**, 1581-1593.

Schneider, K. and Schlegel, H.G. (1976) Purification and properties of soluble hydrogenase from *Alcaligenes eutrophus* H 16. *Biochim. Biophys. Acta*, **452**, 66-80.

Schneider, S., Schmitt, M.O., Brehm, G., Reiher, M., Matousek, P. and Towrie, M. (2003) Fluorescence kinetics of aqueous solutions of tetracycline and its complexes with Mg^{2+} and Ca^{2+}. *Photochem. Photobiol. Sci.*, **2**, 1107-1117.

Schwartz, E., Fritsch, J. and Friedrich, B. (2013) H_2-Metabolizing Prokaryotes. In DeLong, E.F., Lory, S., Stackebrandt, E., Thompson, F. and Rosenberg, E. (eds.), *The Prokaryotes: Prokaryotic Physiology and Biochemistry*. Springer-Verlag, Berlin, pp. 119-199.

Simon, R., Priefer, U. and Pühler. (1983) A broad host range mobilization system for *in vivo* genetic engineering: Transposon mutagenesis in gram negative bacteria. *Nat. Biotechnol.*, 784-791.

Torella, J.P., Gagliardi, C.J., Chen, J.S., Bediako, D.K., Colóna, B., Way, J.C., Silver, P.A. and Nocera, D.G. (2015) Efficient solar-to-fuels production from a hybrid microbial/water-splitting catalyst system. *Proc. Natl. Acad. Sci. U.S.A.*, **112**, 2337-2342.

Wang, E., Bauer, M.C., Rogstam, A., Linse, S., Logan, D.T. and von Wachenfeldt, C. (2008) Structure and functional properties of the *Bacillus subtilis* transcriptional repressor Rex. *Mol. Microbiol.*, **69**, 466-478.

Warburg, O. (1956) On the origin of cancer cells. *Science*, **123**, 309-314.

Williamson, D.H., Lund, P. and Krebs, H.A. (1967) The redox state of free nicotinamide-adenine dinucleotide in the cytoplasm and mitochondria of rat liver. *Biochem. J.*, **103**, 514-527.

Yu, Q. and Heikal, A.A. (2009) Two-photon autofluorescence dynamics imaging reveals sensitivity of intracellular NADH concentration and conformation to cell physiology at the single-cell level. *J. Photochem. Photobiol. B*, **95**, 46-57.

Zhao, Y., Hu, Q., Cheng, F., Su, N., Wang, A., Zou, Y., Hu, H., Chen, X., Zhou, H.M., Huang, X., Yang, K., Zhu, Q., Wang, X., Yi, J., Zhu, L., Qian, X., Chen, L., Tang, Y., Loscalzo, J. and Yang, Y. (2015) SoNar, a Highly Responsive NAD^+/NADH Sensor, Allows High-Throughput Metabolic Screening of Anti-tumor Agents. *Cell Metab.*, **21**, 777-789.

Zhao, Y., Jin, J., Hu, Q., Zhou, H.M., Yi, J., Yu, Z., Xu, L., Wang, X., Yang, Y. and Loscalzo, J. (2011) Genetically encoded fluorescent sensors for intracellular NADH detection. *Cell Metab.*, **14**, 555-566.

Zhou, Y., Wang, L., Yang, F., Lin, X., Zhang, S. and Zhao, Z.K. (2011) Determining the extremes of the cellular NAD(H) level by using an *Escherichia coli* NAD^+-auxotrophic mutant. *Appl. Environ. Microbiol.*, **77**, 6133-6140.